ACS APPLIED MATERIALS & INTERFACES

Research Article

www.acsami.org

Control of Supramolecular Chirality of Nanofibers and Its Effect on Protein Adhesion

Kai Lv, Li Zhang,* Wensheng Lu, and Minghua Liu*

Beijing National Laboratory for Molecular Science, CAS Key Laboratory of Colloid, Interface and Chemical Thermodynamics, Institute of Chemistry, Chinese Academy of Sciences, Beijing 100190, People's Republic of China

Supporting Information

ABSTRACT: Chiral nanostructure, such as the double helix of DNA and α-helix of protein, plays an important role in biochemistry and material sciences. In the organism system, the biological entities always exhibit homochirality and show preference toward one specific enantiomer. How the opposite enantiomers will affect the chirality of the supramolecular nanostructures and their interactions with the biological molecules remains an important issue. In this study, two gelators bearing amphiphilic L-glutamide and D- or L-pantolactone (abbreviated as DPLG and LPLG) were designed, and their self-assembly behavior and interactions with proteins were investigated. It was found that both of the gelators could form gels in the mixed solvent of ethanol and water, and the corresponding gels were characterized with UV−vis spectroscopy, circular dichroism, Fourier transform infrared spectroscopy, X-ray diffraction, and atomic force microscopy. Although both gels formed nanofiber structures and showed many similar properties, their supramolecular chiralities were opposite, which was determined by the chirality of the terminal group. The chirality of the nanofibrous structure is found to influence the protein adhesion significantly. Quartz crystal microbalance technique was used to investigate the adsorption of human serum albumin on the nanofibrous structures. It was revealed that supramolecular nanostructure of DPLG exhibited stronger adhesive ability than that of LPLG, while there is no clear difference at a molecular level. This suggested that slightly different interactions between D and L substances with the biological molecules could be amplified when they formed chiral nanostructures. Molecular dynamic simulations were performed to verify the interaction between the two gelators and protein molecules. A possible model was proposed to explain the interaction between the nanofibers and the proteins.

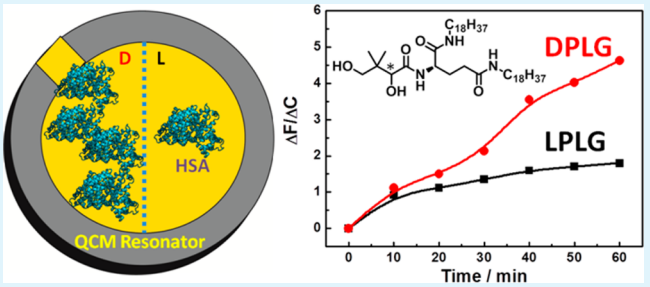

KEYWORDS: *supramolecular chirality, self-assembly, nanofibers, quartz crystal microbalance, human serum albumin, protein adhesion*

INTRODUCTION

Chirality or chiral nanostructure is one of the most fascinating and ubiquitous features commonly found in nature and plays an important role both in biological and material sciences.[1−9] It is well-known that the proteins are composed of L-amino acid but not D-amino acid, while DNA is composed of D-sugar. Such homochirality in the biological system made it vitally important for the construction of the biointerface with certain chirality. When the chiral artificial materials come in contact with biological systems, they interact with each other through such interfaces, and protein adsorption on the biointerface is usually the first event that occurs.[10] Therefore, the functionalized interface with certain chirality and its interactions with the chiral biomolecules has become an important issue.[11−18] In particular, if the materials contain opposite enantiomers or the nanostructures have the opposite chirality, will they influence the properties of the biointerface? So far, several chiral surfaces were constructed through the self-assembled monolayers (SAMs), and their interactions with the biological molecules have been investigated.[19−22] Chiral polymer films have also been proved to be a good platform to realize the protein selective adhesion on the surface,[23−25] which is due to the polymer films having the advantages of easily tailored chemical compositions, properties, and functions.[26−29] However, there is still rarely a report of the protein adhesion on the chiral nanostructures and the control of the chiral surface, which could be very important in the application of the nanomaterials in the biological systems.[30−32]

Supramolecular gel, in which small organic molecules self-assembled into entangled nanostructures to immobilize the solvents, has received increasing attention over the last few decades due to many advantages in constructing biocompatible materials or interfaces.[30−35] One advantage of the gel systems is its easiness to fabricate the chiral nanostructures because many chiral gelators are apt to form gels. The simple gelators were known to form chiral nanostructures, which were controlled by the chirality of the component molecules. Considering the fact that biological molecules usually contain more than one chiral

Received: July 18, 2014
Accepted: October 10, 2014
Published: October 10, 2014

center, a question emerges as to which chiral center determines the chirality of the whole nanostructures if opposite chiral centers were introduced into the molecules.[36,37] Then, how will the formed nanostructures affect the protein adhesion? Previously, we found that L-glutamide amphiphile is a good gelator.[38−40] Moreover, when other moiety was introduced into the structures of the L-glutamide, it can easily form gels. In this study, enantiomeric pantolactone molecules were attached to L-glutamide amphiphile as the terminal groups, and their self-assembly and the chirality of the nanostructures were investigated. It was found that the supramolecular chirality of the formed gel nanofiber was controlled by the terminal group. Then, the effect of the chirality of the nanofiber on the protein adhesion was further investigated.

Various techniques have been used to observe the adhesion and aggregation of biomolecules on the artificial surfaces. Among them, quartz crystal microbalance (QCM) has been widely exploited in the field of chemical and biological sensors because of its many advantages, including intrinsic high sensitivity, low cost, easy installation, and inherent ability to monitor analysis in real time and at ambient temperature.[41−45] With the merits of QCM, it can monitor the small mass changes in real time on a sensor surface. It has the capacity of providing unique information on liposome deposition and fate on various surfaces, so it can record the differences between two chiral enantiomers. Therefore, in recent years, QCM technique has been widely applied in chiral sensing and molecular recognition.[10] By QCM, the adhesion of human serum albumin (HSA) on the chiral nanostructures was investigated. Other techniques such as atomic force microscopes (AFM), circular dichroism (CD) spectra, Fourier transform infrared (FT-IR) spectra, and X-ray diffraction (XRD) were all performed to characterize the basic chiral nanostructures and their interactions with HSA. Finally, molecular dynamics (MD) simulations of the interaction between the gelator and protein molecules were used to generate molecular structures consistent with the results from the QCM experiments. These results offer an important understanding of interactions between the chiral nanostructures and biological entities.

EXPERIMENTAL SECTION

Materials. Compounds D-pantolactone and L-pantolactone were purchased from TCI and used as received. Solvents were purified and dried according to standard methods. ^{1}H NMR spectra were recorded on a Bruker AV400 spectrometer in chloroform ($CDCl_3$) using Me_4Si as internal standard. Mass spectra were determined with BEFLEXIII for the matrix-assisted laser desorption ionization time-of-flight (MALDI-TOF) mass spectrometry (MS) measurements. Elemental analyses were performed on a Carlo-Erba-1106 instrument.

Synthesis of Gelator D(L)PLG. The synthesis of *N*,*N*′-bis-(octadecyl)-L-glutamic diamide (LGAm) was reported previously.[46] The gelator molecules of DPLG and LPLG were synthesized as follows.

Gelator DPLG. D-Pantolactone (0.15g, 1.15 mmol) and LGAm (0.650g, 1.0 mmol) were mixed in a 25 mL flask. The mixture was stirred at 95 °C for ∼6 h. After that, the crude product was dissolved in ethanol (10 mL) and poured into an aqueous saturated solution of NaCl (300 mL). After filtration, the product was purified by recrystallization in ethanol to give a white solid (0.68g, 89.2%). ^{1}H NMR (400 MHz, $CDCl_3$, ppm): δ = 7.60−7.63 (d, 1H), 6.85 (s, 1H), 5.72−5.90 (t, 1H), 4.38−4.43 (m, 1H), 3.99 (s, 1H), 3.45−3.55 (q, 2H), 3.20−3.26 (q, 4H), 1.99−2.40 (m, 4H), 1.49−1.60 (d, 4H), 1.25 (br, 60H), 0.98−1.04 (m, 6H), 0.86−0.89 (t, 6H). MALDI-TOF-MS Calcd for $C_{47}H_{93}N_3O_5$: 779.7. Found: 802.7 $[M + Na]^+$. Anal. Calcd for $C_{47}H_{93}N_3O_5$: C 72.35, H 12.01, N 5.39. Found: C 71.71, H 11.64, N 5.28%.

Gelator LPLG. L-Pantolactone (0.15g, 1.15 mmol) and LGAm (0.650g, 1.0 mmol) were mixed in a 25 mL flask. The mixture was stirred at 95 °C for ∼6 h. After that, the crude product was dissolved in ethanol (10 mL) and poured into an aqueous saturated solution of NaCl (300 mL). After filtration, the product was purified by recrystallization in ethanol to give a white solid (0.65g, 85.3%). ^{1}H NMR (400 MHz, $CDCl_3$, ppm): δ = 7.81−7.84 (d, 1H), 6.82 (s, 1H), 5.87−5.92 (t, 1H), 4.38−4.45 (m, 1H), 4.01 (s, 1H), 3.49−3.51 (q, 2H), 3.22−3.24 (q, 4H), 2.10−2.38 (m, 4H), 1.49−1.60 (d, 4H), 1.25 (br, 60H), 0.98−1.05 (m, 6H), 0.86−0.89 (t, 6H). MALDI-TOF-MS Calcd for $C_{47}H_{93}N_3O_5$: 779.7. Found: 802.7 $[M + Na]^+$. Anal. Calcd for $C_{47}H_{93}N_3O_5$: C 72.35, H 12.01, N 5.39. Found: C 71.91, H 11.83, N 5.30%.

Characterization. The gel formation and their properties were characterized by a series of methods such as AFM; AFM images of the samples were performed in ScanAsyst mode (Dimension FastScan AFM equipped with a fast-scan scanner, Bruker). All the AFM images are shown in height mode without any image processing except flattening. Fourier transform infrared (FT-IR) spectra were recorded on a Bruker Tensor 27 FT-IR spectrometer at room temperature. The single-crystal silica plates were used for FT-IR spectral measurements. UV−vis spectra were measured on a Hitachi U-3900 UV−vis spectrophotometer. The CD spectra were performed on a JASCO-815 spectrometer. The 0.1 mm quartz cells were used for UV−vis and CD measurements. XRD was conducted on a PANalytivcal Empyrean with Cu Kα radiation (λ = 1.5406 Å), which was operated at 40 kV, 40 mA.

QCM Experiment. A cleaned QCM resonator was immersed in a gel of D(L)PLG (6 mg) in the mixed solvent (2 mL, $V_{ethanol}/V_{H_2O}$ = 9:1) for 2 h to produce a thin film on gold substrate. After that, it was rinsed with deionized water sufficiently, dried by infrared lights, and then immersed in a solution of HSA (0.5 mg/mL). The resonator was taken out after 10 min and rinsed with deionized water to remove all the possible impurities that were not adhered to the thin gelator film. We repeated the above process every 10 min and continued for 1 h and collected six data points. We recorded the increased weight every time. As reference, we immersed the QCM resonator into D(L)PLG (1.5 mg) ethanol solution (2.0 mL) to investigate the protein adhesion on molecular surface.

MD Simulations. A 10 ns MD simulation of the complex was carried out with the GROMACS 4.0 package using the GROMOS96 43a1 force field.[47−49] The topology parameters of HSA were created using the GROMACS program. The topology parameters of gelator molecule PLG were built by the Dundee PRODRG2.5 server (beta) and revised. Then the complex was immersed in a cubic box of extended simple point charge (SPC) water molecules. The solvated system was neutralized by adding sodium ions in the simulation, and the entire system was composed of 5882 atoms of HSA, 10 PLG molecules, 14 Na^+ counterions, and different solvent atoms in DPLG and LPLG systems.

RESULTS AND DISCUSSION

Gel Formation. The gelation was performed in the mixed solvents of EtOH/H_2O (v/v = 9:1) and confirmed by the "stable to the inversion of a test tube" method. The concentration of the gel was 3.9 mM. The gel can be fabricated by two methods. One is by adding the gelator and mixed solvents in a screw-capped sample tube and then heating to a transparent solution. After the transparent solution was cooled to room temperature, the gel was formed and confirmed by the inverted test tube method, as shown in Figure 1B. In the other method, we can first dissolve the gelator molecules into the EtOH. The addition of water into the solution caused an instant gelation.[50] Because diffusion of the water into the solvent in the instant gelation can cause some inhomogeneity,

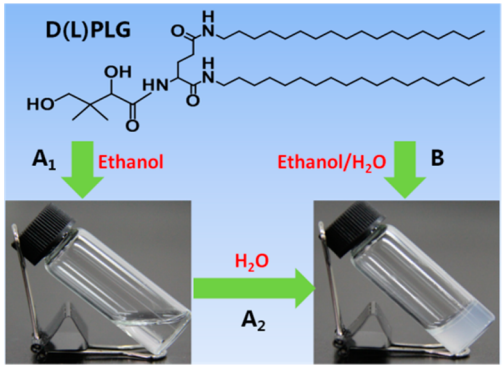

Figure 1. Molecular structure of the gelator D(L)PLG and two different ways to get the gelation. Method A: The gelator molecules were dissolved in the EtOH first (A_1), and then the addition of water into the solution caused an instant gelation (A_2). Method B: The gelator molecules were dissolved in the mixed solvents by heating, and then the gel was formed after the transparent solution cooled to room temperature.

we used the heating and cooling cycle to fabricate the gel in the following experiments.

The morphology of the gels of DPLG and LPLG in EtOH/H_2O was investigated by AFM, as shown in Figure 2.

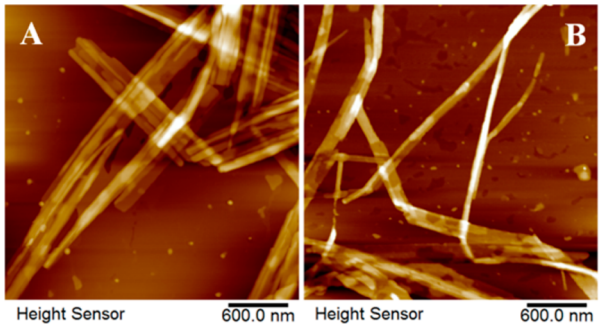

Figure 2. AFM images of (A) DPLG and (B) LPLG xerogels from EtOH/H_2O (v/v = 9:1).

Disordered fibers were obtained for both DPLG and LPLG xerogels. The nanofiber structures with a width of 110−150 nm and a length of several micrometers were found for the DPLG xerogels obtained from EtOH/H_2O system, while the LPLG has little differences with the nanofiber width of 70−100 nm. Both of these two nanofibers were very slender, and some of the fibers bundled together to form thick structures, which can be seen from the AFM images.

To gain further insight into the structures of these two self-assemblies, we performed XRD measurements. Figure 3A shows the XRD patterns of the xerogels obtained from EtOH/H_2O. There were two diffraction peaks corresponding to the *d* spacings of 3.68 and 1.84 nm. The *d* spacing ratio of 1:0.5 was consistent with a lamellar structure. The length of 3.68 nm was larger than the extended molecular length of D(L)PLG (3.2 nm estimated from the CPK molecular model) but smaller than twice the length, thus suggesting that the gelator molecules self-assembled into a bilayer structure with interdigitated aliphatic tails, in which the amide moieties organized into a well-defined arrangement through strong hydrogen-bonding interactions, and the head-groups exhibited intermolecular hydrogen-bonding interactions with neighboring molecules, as illustrated in Figure 3B.

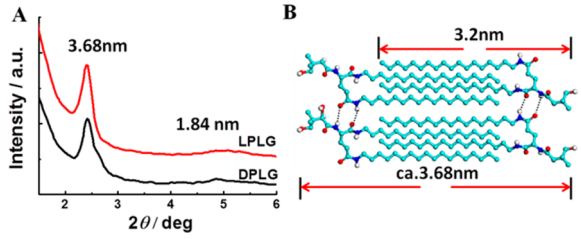

Figure 3. (A) XRD patterns of DPLG and LPLG xerogels and (B) the model for the gelator arrangements in the EtOH/H_2O gel with an interdigitated bilayer structure. The dashed line represents the hydrogen bond.

Supramolecular Chirality of the Nanofibers. Because these gelators have two chiral centers, we measured the CD spectra to see if there is any difference in the chirality of the gels, as shown in Figure 4. In solution, these compounds did

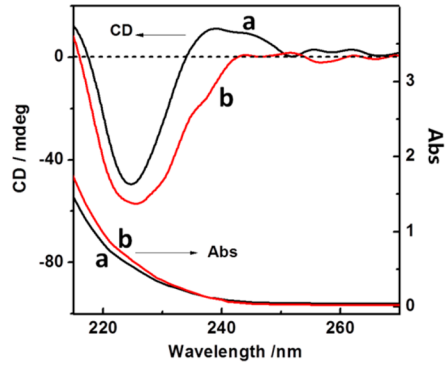

Figure 4. CD and UV−vis spectra of (a) DPLG gel and (b) LPLG gel in EtOH/H_2O (v/v = 9:1).

not show any CD signals (Figure S1, Supporting Information) because the gelators did not form chiral supramolecular structures. For the DPLG gel, a positive Cotton effect at 240 nm and a negative band at 226 nm with a crossover at 235 nm were observed. For the LPLG gel, there was one negative Cotton effect at 238 nm but with a broad band. This clearly indicated that the terminal groups affect the chirality of the gels. In the case of DPLG organogels, a positive supramolecular chirality with exciton coupling was found, while the negative one was observed at LPLG. Taking into account the configuration of the DPLG or LPLG, the obvious difference in supramolecular chirality was speculated as coming from the terminal group of gelators. Moreover, a notable exciton coupling of CD signals for DPLG indicated that the intermolecular arrangement and interactions between DPLG molecules were different from those of LPLG.

Protein Adsorption on the Gel Nanofibers. To gain the insight of the formed chiral nanofibers on the protein adhesion, QCM measurements were performed to detect the protein adsorption. A series of surfaces with supramolecular architectures were prepared, as illustrated in Figure S2 (Supporting Information). The detailed steps were described in the Experimental Section.

Figure 5 shows the time-dependent curves of ΔF on LPLG and DPLG resonators using a flow of HSA solution (0.5 mg/mL). Interestingly, a significant difference in HSA adsorption on PLG supramolecular structures was observed. For the LPLG nanofibers (Figure 5A, curve b), an adsorption terrace appears

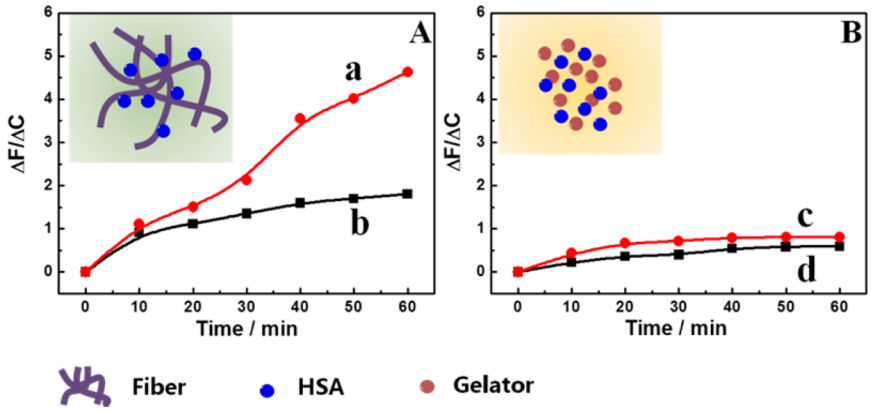

Figure 5. Time-dependent curves of frequency change in QCM experiments. (A) HSA molecules interacted with supramolecular assembly structure (a, DPLG; b, LPLG) and (B) HSA molecules interacted with gelator molecules (c, DPLG; d, LPLG). (Inset) The adsorption model for the HSA with (A) fibrous structure and (B) the gelator molecules.

at about 20 min, but for the DPLG system, there is no adsorption terrace appearing after 20 min. On the contrary, the adsorption continues to increase as time goes on. It clearly shows that HSA exhibits a stronger adsorption on the DPLG supramolecular structure than that on the LPLG, indicating that the supramolecular chirality strongly influences the protein adsorption dynamics. Compared with the supramolecular structure (gel state), the same experiment was done with the gelator molecules (solution state). As can be seen from the curves in Figure 5, there is an obvious difference between supramolecular nanostructures and molecular systems. The nanostructures of DPLG exhibit a stronger adsorption. The network structure might provide more acting sides for HSA molecules, as shown in the inset of Figure 5A. There is almost no obvious difference for protein adsorption on DPLG or LPLG monomer surface (Figure 5B), further supporting that the supramolecular structure has a distinct effect on protein adsorption.

Characterization of the Cogel System: Gelator and HSA. To investigate the interaction between the gel nanostructure and HSA, we followed various characterization methods. Figure S3 (Supporting Information) shows the corresponding AFM images of the Cogel. Compared to the DPLG and LPLG in EtOH/H_2O (Figure 2), the fibers in the Cogel systems were very tenuous and aggregated together to form a wide band. This indicated that the HSA can interact with the gelator molecules and form the Cogel in EtOH/H_2O. The belt formed in DPLG + HSA is a little wider than that in LPLG + HSA, which is in agreement with the data of the QCM part.

The FT-IR spectra were performed to investigate the interaction between the HSA and the gelator molecules, as shown in Figure 6. First, both the gels of DPLG and LPLG showed strong vibration bands at 3293, 1642, and 1559 cm^{-1}, which could be ascribed to the N−H vibrations of amide I and amide II, respectively. This showed that the gelator molecules form the gels with strong H-bond interactions. Upon reacting with the protein HSA, there are slight changes and differences in the FT-IR spectra. After interaction with the HSA, a broad shoulder peak around 3500 cm^{-1} was found in the DPLG−HSA and LPLG−HSA assemblies, which can be also ascribed to the H-bond formation between the HSA and gelator molecules. This explicitly indicated that the HSA molecules can be adhered to the gelator molecules with the help of H-bond.

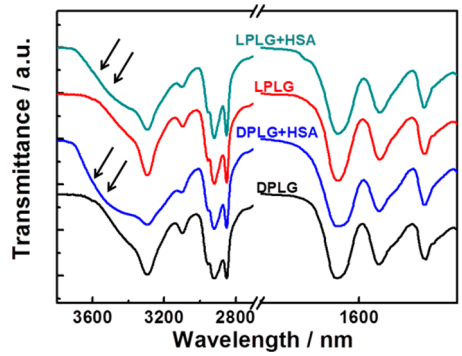

Figure 6. FT-IR spectra of the xerogels of (top to bottom) LPLG + HSA, LPLG, DPLG + HSA, and DPLG.

For the LPLG, it displays a narrow spectral profile with a full width half-maximum (fwhm) of ∼250 cm^{-1}, and after adsorption the HSA molecules, the fwhm changed to ∼430 cm^{-1}. In comparison, the fwhm of DPLG show ∼285 and ∼580 cm^{-1} before and after adsorpted the HSA molecules, respectively. These changes indicate that HSA molecules interacted with gelators via the formation of H-bonds, leading to the broadening of vibration band. In addition, a broadening of the amide I peak was observed for DPLG−HSA, indicating the DPLG nanostructure has good adsorption ability to the HSA molecules. These results are in good accordance with the QCM experiments.

The CD spectra of the supramolecular nanostructure after protein adsorption were also taken (Figure 7). After the xerogels of DPLG and LPLG immersed into the HSA solution for 60 h, the adsorption peak at 220 nm increased more for DPLG than that for LPLG xerogels. These results are in good agreement with the QCM data shown above, and prove that the DPLG supramolecular structure exhibited stronger adsorption ability than LPLG.

DISCUSSION

From the results above, we can conclude that the chiral supramolecular structures exhibit enantioselective adhesion to HSA molecules. The possible scheme of the enantioselective recognition of nanostructures to HSA is shown in Figure 8A. The gelator LPLG and DPLG molecules can self-assemble into fiber structures in the mixed ethanol and H_2O with a volume ratio 9:1. During the formation of the fiber structure, the

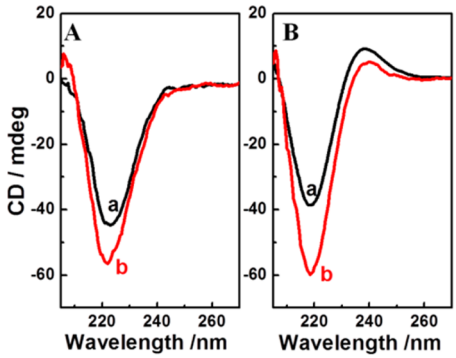

Figure 7. CD spectra of the xerogel of (A) LPLG and (B) DPLG (a) before and (b) after immersion into the HSA solution for 60 h.

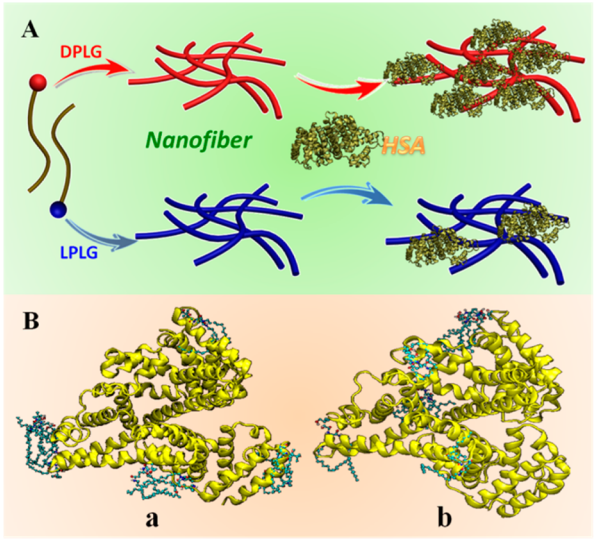

Figure 8. (A) Different adhesion abilities of nanomaterials based on HSA and gelator molecule interactions. (B) The final simulation conformations of the HSA and gelator molecules (a) LPLG and (b) DPLG. (Pictures generated with VMD,[51] gelator molecules as CPK model, and HSA as NewCartoon; (light blue) gelator molecules, (red spheres) oxygen atoms in gelator molecules, and (yellow) HSA molecules.)

intermolecular hydrogen-bonding interactions between the amide group and hydroxyl group and the hydrophobic interactions played important roles in bringing the gelator molecules to align together. The XRD analysis of the supramolecular gels showed that the gelator molecules self-assembled into a bilayer structure with interdigitated aliphatic tails. These supramolecular structures with different chirality exhibited chiral recognition performance on the protein adsorption process. This process can be verified by the QCM experiments. With the help of hydrogen bonding and hydrophobic interactions between the gelator and protein molecules, the proteins exhibit a stronger adsorption on the DPLG supramolecular structure than that of the LPLG.

Supramolecular chirality of the organogels is the chirality of assembled aggregates transferred from molecular chirality. It is related to the assembly model of gelator molecules. Therefore, chirality is intrinsically present in gelator structure at both the molecular and supramolecular levels, and it plays a decisive role in the interaction with other biochemical species. To further investigate and understand the interaction between the gelator and HSA molecules, we further used molecular dynamics calculations to simulate the molecular configurations of gelator molecules and HSA molecules in an aqueous environment, in which the GROMACS program was selected for the simulation. Figure 8B shows the final simulation conformations of the HSA and gelator molecules. In the LPLG/HSA system, after 10 ns MD simulation, the gelator molecules can self-assemble into some small clusters and re-adhere to the periphery of the HSA molecule (Figure 8B,a). On the contrary, the DPLG molecules can penetrate into the protein molecules. From Figure 8B,b we can see some of the DPLG molecules can work closely together with HSA molecule through the long chain entanglement. At a molecular level, the chiral molecules showed slightly different interactions with protein molecules. But such slight a difference could not be detected in an ordinary way at a molecular level. However, when they formed chiral nanostructures, such a difference was significantly amplified, and we could detect them clearly from CD spectra and QCM experiments. Because the DPLG molecules have better ability to interact with HSA molecules compared with LPLG, the supramolecular structures of DPLG molecules could achieve more quality molecular adsorption of HSA.

CONCLUSION

In conclusion, two amphiphilic gelators bearing two chiral centers were found to form organogels in the mixed solvents of ethanol and water. They formed chiral nanofibers with the opposite supramolecular chirality, in which the terminal group determined the whole chirality of the nanofiber. The chiral nanofibers showed different adhesion abilities of the protein, and DPLG nanofiber exhibited stronger adsorption ability than LPLG, which can be verified by QCM detection, CD spectral measurements, and the molecular dynamics simulation. This study demonstrated that enantiomers with different chirality may show different interactions with the biological molecules, and this difference can be significantly amplified upon forming the chiral nanostructures with opposite chirality.

ASSOCIATED CONTENT

Supporting Information

CD spectra of DPLG and LPLG solutions, preparation scheme of QCM experiments, and AFM images of DPLG + HSA and LPLG + HSA xerogels. This material is available free of charge via the Internet at http://pubs.acs.org.

AUTHOR INFORMATION

Corresponding Authors

*E-mail: liumh@iccas.ac.cn.
*E-mail: zhangli@iccas.ac.cn.

Notes

The authors declare no competing financial interest.

ACKNOWLEDGMENTS

The authors are grateful to the Basic Research Development Program (2013CB834504), the National Natural Science Foundation of China (Nos. 91027042, 21021003, and 21227802), and the Strategic Priority Research Program of the Chinese Academy of Sciences (Grant No. XDB12020200).

REFERENCES

(1) Che, S.; Liu, Z.; Ohsuna, T.; Sakamoto, K.; Terasakl, O.; Tatsuml, T. Synthesis and Characterization of Chiral Mesoporous Silica. *Nature* **2004**, *429*, 281−284.

(2) Bentley, R. Role of Sulfur Chirality in the Chemical Processes of Biology. *Chem. Soc. Rev.* **2005**, *34*, 609−624.
(3) Akazaki, K.; Toshimitsu, F.; Ozawa, H.; Fujigaya, T.; Nakashima, N. Recognition and One-Pot Extraction of Right- and Left-Handed Semiconducting Single-walled Carbon Nanotube Enantiomers using Fluorene−Binaphthol Chiral Copolymers. *J. Am. Chem. Soc.* **2012**, *134*, 12700−12707.
(4) Wang, Y.; Xu, J.; Wang, Y.; Chen, H. Emerging Chirality in Nanoscience. *Chem. Soc. Rev.* **2013**, *42*, 2930−2962.
(5) Yao, X.; Hu, Y. W.; Cao, B.; Peng, R.; Ding, J. D. Effects of Surface Molecular Chirality on Adhesion and Differentiation of Stem Cells. *Biomaterials* **2013**, *34*, 9001−9009.
(6) Tkachenko, G.; Brasselet, E. Optofluidic Sorting of Material Chirality by Chiral Light. *Nat. Commun.* **2014**, *5*, 3577.
(7) Qing, G. Y.; Sun, T. L. Chirality-Driven Wettability Switching and Mass Transfer. *Angew. Chem., Int. Ed.* **2014**, *53*, 930−932.
(8) Lara, C.; Reynolds, N. P.; Berryman, J. T.; Xu, A.; Zhang, A.; Mezzenga, R. ILQINS Hexapeptide, Identified in Lysozyme Left-Handed Helical Ribbons and Nanotubes, Forms Right-Handed Helical Ribbons and Crystals. *J. Am. Chem. Soc.* **2014**, *136*, 4732−4739.
(9) Zhang, L.; Qin, L.; Wang, X. F.; Cao, H.; Liu, M. H. Supramolecular Chirality in Self-Assembled Soft Materials: Regulation of Chiral Nanostructures and Chiral Functions. *Adv. Mater.* **2014**, DOI: 10.1002/adma.201305422.
(10) Wang, X.; Gan, H.; Sun, T. L. Chiral Design for Polymeric Biointerface: The Influence of Surface Chirality on Protein Adsorption. *Adv. Funct. Mater.* **2011**, *21*, 3276−3281.
(11) Geva, M.; Frolow, F.; Eisenstein, M.; Addadi, L. Antibody Recognition of Chiral Surfaces. Enantiomorphous Crystals of Leucine−Leucine−Tyrosine. *J. Am. Chem. Soc.* **2003**, *125*, 696−704.
(12) Somorjai, G. A.; Frei, H.; Park, J. Y. Advancing the Frontiers in Nanocatalysis, Biointerfaces, and Renewable Energy Conversion by Innovations of Surface Techniques. *J. Am. Chem. Soc.* **2009**, *131*, 16589−16605.
(13) Hynes, R. O. The Extracellular Matrix: Not Just Pretty Fibrils. *Science* **2009**, *326*, 1216−1219.
(14) Wang, X.; Gan, H.; Sun, T. L.; Su, B. L.; Fuchs, H.; Vestweber, D.; Butz, S. Stereochemistry Triggered Differential Cell Behaviours on Chiral Polymer Surfaces. *Soft Matter* **2010**, *6*, 3851−3855.
(15) Zhou, F.; Yuan, L.; Li, D.; Huang, H.; Sun, T. L.; Chen, H. Cell Adhesion on Chiral Surface: The Role of Protein Adsorption. *Colloids Surf., B* **2012**, *90*, 97−101.
(16) El-Gindi, J.; Benson, K.; Cola, L. D.; Galla, H. J.; Kehr, N. S. Cell Adhesion Behavior on Enantiomerically Functionalized Zeolite L Monolayers. *Angew. Chem., Int. Ed.* **2012**, *51*, 3716−3720.
(17) González-Campo, A.; Amabilino, D. B. Biomolecules at Interfaces: Chiral, Naturally. *Top. Curr. Chem.* **2013**, *333*, 109−156.
(18) Zhang, M. X.; Qing, G. Y.; Sun, T. L. Chiral Biointerface Materials. *Chem. Soc. Rev.* **2012**, *41*, 1972−1984.
(19) Love, J. C.; Estroff, L. A.; Kriebel, J. K.; Nuzzo, R. G.; Whitesides, G. M. Self-Assembled Monolayers of Thiolates on Metals as a Form of Nanotechnology. *Chem. Rev.* **2005**, *105*, 1103−1169.
(20) Arima, Y.; Iwata, H. Effect of Wettability and Surface Functional Groups on Protein Adsorption and Cell Adhesion using Well-Defined Mixed Self-Assembled Monolayers. *Biomaterials* **2007**, *28*, 3074−3082.
(21) Beilis, E.; Belgorodsky, B.; Fadeev, L.; Cohen, H.; Richter, S. Surface-Induced Conformational Changes in Doped Bovine Serum Albumin Self-Assembled Monolayers. *J. Am. Chem. Soc.* **2014**, *136*, 6151−6154.
(22) Sun, T. L.; Han, D.; Rhemann, K.; Chi, L. F.; Fuchs, H. Stereospecific Interaction Between Immune Cells and Chiral Surfaces. *J. Am. Chem. Soc.* **2007**, *129*, 1496−1497.
(23) Ratner, B. D.; Bryant, S. J. Biomaterials: Where We have Been and Where We are Going. *Annu. Rev. Biomed. Eng.* **2004**, *6*, 41−75.
(24) Senaratne, W.; Andruzzi, L.; Ober, C. K. Self-Assembled Monolayers and Polymer Brushes in Biotechnology: Current Applications and Future Perspectives. *Biomacromolecules* **2005**, *6*, 2427−2448.
(25) Wang, X.; Gan, H.; Zhang, M. X.; Sun, T. L. Modulating Cell Behaviors on Chiral Polymer Brush Films with Different Hydrophobic Side Groups. *Langmuir* **2012**, *28*, 2791−2798.
(26) Tugulu, S.; Silacci, P.; Stergiopulos, N.; Klok, H. A. RGD-Functionalized Polymer Brushes as Substrates for the Integrin Specific Adhesion of Human Umbilical Vein Endothelial Cells. *Biomaterials* **2007**, *28*, 2536−2546.
(27) Mizutani, A.; Kikuchi, A.; Yamato, M.; Kanazawa, H.; Okano, T. Preparation of Thermoresponsive Polymer Brush Surfaces and Their Interaction with Cells. *Biomaterials* **2008**, *29*, 2073−2081.
(28) Brun-Graeppi, A. K. A. S.; Richard, C.; Bessodes, M.; Scherman, D.; Merten, O.-W. Thermoresponsive Surfaces for Cell Culture and Enzyme-Free Cell Detachment. *Prog. Polym. Sci.* **2010**, *35*, 1311−1324.
(29) Wischerhoff, E.; Uhlig, K.; Lankenau, A.; Börner, H. G.; Laschewsky, A.; Duschl, C.; Lutz, J.-F. Controlled Cell Adhesion on PEG-based Switchable Surfaces. *Angew. Chem., Int. Ed.* **2008**, *47*, 5666−5668.
(30) Luo, Z. L.; Zhang, S. G. Designer Nanomaterials using Chiral Self-Assembling Peptide Systems and Their Emerging Benefit for Society. *Chem. Soc. Rev.* **2012**, *41*, 4736−4754.
(31) Luo, Z. L.; Yue, Y. Y.; Zhang, Y. F.; Yuan, X.; Gong, J. P.; Wang, L. L.; He, B.; Liu, Z.; Sun, Y. L.; Liu, J.; Hu, M. F.; Zheng, J. Designer D-Form Self-Assembling Peptide Nanofiber Scaffolds for 3-Dimensional Cell Cultures. *Biomaterials* **2013**, *34*, 4902−4913.
(32) Liu, G. F.; Zhang, D.; Feng, C. L. Control of Three-Dimensional Cell Adhesion by the Chirality of Nanofibers in Hydrogels. *Angew. Chem., Int. Ed.* **2014**, *53* (30), 7789−7793.
(33) Cushing, M. C.; Anseth, K. S. Hydrogel Cell Cultures. *Science* **2007**, *316*, 1133−1134.
(34) Xia, Y. Q.; Gu, Y. F.; Zhou, X.; Xu, H.; Zhao, X. B.; Yaseen, M.; Lu, J. R. Controllable Stabilization of Poly(*N*-isopropylacrylamide)-based Microgel Films through Biomimetic Mineralization of Calcium Carbonate. *Biomacromolecules* **2012**, *13*, 2299−2308.
(35) Dou, X. Q.; Li, P.; Zhang, D.; Feng, C. L. RGD Anchored C_2-Benzene based PEG-like Hydrogels as Scafolds for Two and Three Dimensional Cell Cultures. *J. Mater. Chem. B* **2013**, *1*, 3562−3568.
(36) Vujičić, N. Š.; Glasovac, Z.; Zweep, N.; van Esch, J. H.; Vinković, M.; Popovic, J.; Žinić, M. Chiral Hexa- and Nonamethylene-Bridged Bis(L-leu-oxalamide) Gelators: The First Oxalamide Gels Containing Aggregates with a Chiral Morphology. *Chem.—Eur. J.* **2013**, *19*, 8558−8572.
(37) Fu, Y. T.; Li, B. Z.; Huang, Z. B.; Li, Y.; Yang, Y. G. Terminal is Important for the Helicity of the Self-assemblies of Dipeptides Derived from Alanine. *Langmuir* **2013**, *29*, 6013−6017.
(38) Duan, P. F.; Liu, M. H. Design and Self-Assembly of L-Glutamate-based Aromatic Dendrons as Ambidextrous Gelators of Water and Organic Solvents. *Langmuir* **2009**, *25*, 8706−8713.
(39) Zhu, X. F.; Li, Y. G.; Duan, P. F.; Liu, M. H. Self-Assembled Ultralong Chiral Nanotubes and Tuning of Their Chirality Through the Mixing of Enantiomeric Components. *Chem.—Eur. J.* **2010**, *16*, 8034−8040.
(40) Duan, P. F.; Li, Y. G.; Li, L. C.; Deng, J. G.; Liu, M. H. Multiresponsive Chiroptical Switch of an Azobenzene-Containing Lipid: Solvent, Temperature, and Photoregulated Supramolecular Chirality. *J. Phys. Chem. B* **2011**, *115*, 3322−3329.
(41) Yang, M. Q.; He, J. H. Tailoring the Structure of Metal Oxide Nanostructures towards Enhanced Sensing Properties for Environmental Applications. *J. Colloid Interface Sci.* **2012**, *368*, 41−48.
(42) Volden, S.; Eilertsen, J. L.; Singh, G.; Wang, W.; Zhu, K. Z.; Nyström, B.; Glomm, W. R. Effect of Charge Density Matching on the Temperature Response of PNIPAAM Block Copolymer−Gold Nanoparticles. *J. Phys. Chem. C* **2012**, *116*, 12844−12853.
(43) Alf, M. E.; Hatton, T. A.; Gleason, K. K. Insights into Thin, Thermally Responsive Polymer Layers through Quartz Crystal Microbalance with Dissipation. *Langmuir* **2011**, *27*, 10691−10698.
(44) Lind, T. K.; Zielińska, P.; Wacklin, H. P.; Urbańczyk-Lipkowska, Z.; Cárdenas, M. Continuous Flow Atomic Force Microscopy Imaging Reveals Fluidity and Time-Dependent Interactions of Antimicrobial

Dendrimer with Model Lipid Membranes. *ACS Nano* **2014**, *8*, 396−408.
(45) Wang, C.; Qian, C.; Roman, M.; Glasser, W. G.; Esker, A. R. Surface-Initiated Dehydrogenative Polymerization of Monolignols: A Quartz Crystal Microbalance with Dissipation Monitoring and Atomic Force Microscopy Study. *Biomacromolecules* **2013**, *14*, 3964−3972.
(46) Zhu, X. F.; Li, Y. G.; Duan, P. F.; Liu, M. H. Self-Assembled Ultralong Chiral Nanotubes and Tuning of Their Chirality Through the Mixing of Enantiomeric Components. *Chem.—Eur. J.* **2010**, *16*, 8034−8040.
(47) Lindahl, E.; Hess, B.; van der Spoel, D. GROMACS 3.0: A Package for Molecular Simulation and Trajectory Analysis. *J. Mol. Model.* **2001**, *7*, 306−317.
(48) Sudhamalla, B.; Gokara, M.; Ahalawat, N.; Amooru, D. G.; Subramanyam, R. Molecular Dynamics Simulation and Binding Studies of β-Sitosterol with Human Serum Albumin and Its Biological Relevance. *J. Phys. Chem. B* **2010**, *114*, 9054−9062.
(49) Van Gunsteren, W. F.; Billeter, S. R.; Eising, A. A.; Hünenberger, P. H.; Krüger, P. K. H. C.; Mark, A. E.; Scott, W. R. P.; Tironi, I. G. *Biomolecular Simulation: The GROMOS96 Manual and User Guide;* Vdf Hochschulverlag AG an der ETH Zürich: Zürich, Switzerland, 1996.
(50) Cao, H.; Duan, P. F.; Zhu, X. F.; Jiang, J.; Liu, M. H. Self-Assembled Organic Nanotubes Through Instant Gelation and Universal Capacity for Guest Molecule Encapsulation. *Chem.—Eur. J.* **2012**, *18*, 5546−5550.
(51) Humphrey, W.; Dalke, A.; Schulten, K. VMD: Visual Molecular Dynamics. *J. Mol. Graphics* **1996**, *14*, 33−38.